2021

Effect of Surface Wettability on Droplets Growth during Water Condensation and Initial Droplets Icing

Fuqiang Ren
Auburn University, lzc0047@auburn.edu

Ellyn Harges

Lorenzo Cremaschi

Effect of Surface Wettability on Droplets Growth during Water Condensation and Initial Droplets Icing

Fuqiang REN[1], Ellyn HARGES[1], Lorenzo CREMASCHI[1]*

[1]Auburn University, Department of Mechanical Engineering,
Auburn, Alabama, United States
Phone: (334) 844-3302
Email: lzc0047@auburn.edu

* Corresponding Author

ABSTRACT

Air-source heat pump systems extract heat directly from the cold outdoor ambient and reject heat to the warm indoor environments of residential and commercial buildings. During their winter operation, the outdoor coil often accumulates frost on its surface. Frost acts as an insulator and blocks air passages, reducing the heat transfer rate and increasing the pressure drop of air passing through the coil. Defrost cycles are periodically executed between the heating times to melt the ice, drain the water from the outdoor coil, and free accumulated frost before the heating service can start again. Unfortunately, too many defrost cycles penalize the efficiency of the heat pumps.

Most research in frost mitigation focused on superhydrophobic surfaces, lubricant impregnated surfaces, and nanostructured surfaces. Some studies proposed surface types that would lower ice adhesion such that droplet removal was promoted before freezing. However, the mitigation effects of these surfaces can be sensitive to experimental conditions and surface structure. Additionally, in circumstances where frost formation cannot be prevented due to the operating conditions, the challenge of predicting frost nucleation and growth rate is further complicated by transient flow conditions with combined heat and mass transfer phenomena to moving frost boundaries.

This paper presents new data of freezing time, droplet diameter, and droplet shape with different surface wettability during initial droplet icing. Water condensation and icing formed on the flat plates for convective channel flows. Four surfaces with different wettability were investigated under two test conditions. The contact angle ranged from less than 10 degrees (i.e., superhydrophilic) to over 109 degrees (i.e., hydrophobic). Two surfaces shared similar contact angles but had different coating components. Because frost nucleation was partially a stochastic phenomenon subjected to many variables that were difficult to control and replicate even in a laboratory setting, frost tests with identical environmental and surface temperature conditions were repeated several times to gather meaningful averages for the freezing time and to quantify the magnitude of potential variability in the frost nucleation time and droplets size due to the surface wettability characteristics. The new data presented in this paper are used to inform and validate physics-based frost models, predicting the nucleation features and actual frost formation time for coated fin structures of heat exchangers.

Keywords: freezing time, water condensation, nucleation, repeatability, fin coatings, heat exchangers

1. INTRODUCTION

Air-source heat pump systems extract heat directly from the cold outdoor ambient and reject heat to the warm indoor environments of residential and commercial buildings. The performances of these systems are dependent on the air conditions of the outdoor environments. During winter operations, the outdoor coils often accumulate frost on their surfaces. Frost acts as an insulator and blocks air passages, reducing the heat transfer rate and increasing the pressure drop of air passing through the coils. These two combined effects lead to an increase in the temperature difference between the evaporating refrigerant and the outdoor air. This phenomenon enhances frost formation and, at the same

time, lowers the coefficient of performance of the heat pump. Defrost cycles are periodically executed in between the heating times to melt the ice, drain the water from the outdoor coils, and free accumulated frost before the heating service can start again. Unfortunately, defrost cycles penalize the efficiency of heat pumps, and their frequency should be monitored and controlled. One potential means of reducing the number of defrost cycles is to utilize particular surface types or chemical surface coatings on the heat exchangers' fin structures.

For environmental conditions typical of a heat pump operating conditions, frost formation has three stages: the droplet condensation and growth stage, the crystal growth stage, and the frost full layer growth stage (Hoke et al., 2000). All stages are sensitive to surface temperature, air temperature, humidity ratio, and air velocity. Besides these variables, droplet growth rate and the onset of freezing depend on the surface wettability, at least to some extent. Tao et al. (1993) observed frost growth consisting of two stages. The first stage was liquid droplet growth and the second stage was ice crystal growth. The transition time between the two stages was meaningful for numerical modeling of frost formation. Sheng et al. (2020) presented droplet shapes and wet area coverage on different surface types and observed that the results for superhydrophobic surfaces were different from those for a hydrophobic surface. They also indicated that droplets on a hydrophilic surface had extensive wet area coverage and larger water droplets. Kim et al. (2016) suggested that the radius of the droplets on a surface increased due to two droplets merging. Hoke et al. (2000) observed that smaller and more uniform droplets were formed if cold substrate temperature decreased. Seki et al. (1985) utilized two different test plates having contact angles of 110° and 43°. Frost incipient phenomena showed that droplets on the 43° plate were larger than those with a large contact angle. Bryant (1995) observed that a hydrophobic coating delayed the onset of ice nucleation by 15 to 35%, and the additional time allowed 15 to 25% more water condensation on the surface before the droplets froze. Adanur et al. (2019) investigated the effect of biphilic coatings with regions of hydrophilic coatings adjacent to areas with hydrophobic coatings. Their investigation indicated that this kind of surface wettability could influence the droplet movement and delay freezing. Harges et al. (2020) investigated the effects of surface wettability under different test conditions. The average droplets distribution and average diameter were also presented. Kim et al. (2015) had 10 repeated tests for each contact angle from 70° to 160°. The uncertainties of the frosting time of their 10 repeated tests had a maximum of 9.5%. They concluded that when test plate temperature was -10°C (14°F) and -12°C (10.4°F), the dimensionless freezing time increased with increasing water contact angle, while when test plate temperature was -10°C, it did not have an effect on freezing time retardation.

This paper is based on the authors' previous work (Cremaschi et al., 2018), and it presents new data on droplet growth and freezing characteristics during initial frost nucleation. The central regions of the test plates were visually recorded by an in-situ calibrated non-invasive infrared thermal camera to provide instantaneous measurements of droplet diameter and droplet area coverage, as well as droplet freezing time. The IR camera also measured the frost surface temperature while the test apparatus measured the instantaneous heat flux and water mass deposited on the cold flat plates. With respect to the authors' previous study (Cremaschi et al., 2018), the static contact angle of flat plates was extended and ranged from less than 10° (i.e., superhydrophilic) to over 109° (i.e., hydrophobic). Because frost nucleation was partially a stochastic phenomenon subject to many variables that were difficult to control and replicate even in a laboratory setting, frost tests with identical environmental and surface temperature conditions were repeated several times in different days and sometimes different months. This approach quantified the effect of surface coating robustness, that is, potential coating deterioration and potential surface oxidations due to multiple frost and defrost processes, cleanups, and water drying procedures. Averages and distributions of the experiments are discussed in this paper. The variability of the frost nucleation time and droplets diameter at the onset of freezing are also presented and analyzed based on the surface wettability characteristics of newly coated surfaces.

2. EXPERIMENTAL METHODOLOGY

2.1 Experimental Test Apparatus
The experimental facility, test setup, sensors, and data reduction are described in detail in the authors' previous work (Adanur et al., 2019). They are briefly summarized next for completeness of this paper. In addition, the cleaning and drying procedures used during the tests were described in detail in Harges et al. (2020).

The test facility consisted of a closed airflow wind tunnel that controlled the air temperature, humidity, and speed. A second smaller airflow wind tunnel, shown in Figure 1(a), was installed inside the large wind tunnel, and it accommodated the cold flat plates. Two thermoelectric coolers (TECs) and an in-house built stainless-steel heat flux meter controlled the test plates' surface temperature during frosting. An infrared (IR) camera was positioned at the top of the plate, and a High Resolution Charged Couple Device (HR CCD) camera was located at the front or, in repeated tests, at the side of the test plate, as shown in Figure 1(b). The IR camera measured the temperature of the frost surface and droplet size during freezing, while the HR CCD camera measured droplet size right after freezing

and subsequent frost thickness. Sensors of the test apparatus shown in Figure 1(a) measured the time-dependent heat flux, surface temperature, air dry bulb, and dew point temperatures at the inlet and outlet of the test plates, airflow rate, and air static pressure and air pressure drop across the channel of the test plate. We installed smoothly converging and diverging duct sections at the inlet and outlet of the test plate, keeping the angles low enough to reasonably assume the airflow over the plate to be initially well mixed and fully developed. These converging and diverging sections to and from the test plate sections are indicated in Figure 1(a). Aluminum plates were machined to dimensions of 25mm length (i.e., depth of the plate along the airflow direction) by 152 mm width and 6 mm thickness (1 in x 6 in. x 0.25 in). These plates are referred to as the "test plates" throughout this paper. The test plates were exposed to convective airflow frosting conditions on their top surfaces with airflow cross-section dimensions of 4 mm high (perpendicular to the surface) and 152 mm wide (equal to the width of the test section). Air entered the test plates at 5°C (41°F) dry bulb temperature and the dew point temperature was 2°C (35.5°F), which yielded an entering relative humidity of about 80% and absolute humidity of 0.0043 kg-water/kg-air. In order to maintain the dew point temperature constant at the inlet, a humidifier was utilized with purified deionized water (Water, ACS Reagent Grad, ASTM Type I, ASTM Type II). The airflow rate (4.9 CFM) was constant for the entire test, that is, during both phases of frost nucleation and subsequent frost growth. During a frost test, a nitrogen displacement technique was used to produce ultra-low dew point temperatures in the gas surrounding the test plate during the temperature pull-down period of the test plate. This nitrogen blanket avoided water vapor condensation (and frost nucleation) during the pull-down phase of the test. Then, when the test plate temperature reached the setpoint, nitrogen gas was removed, and the air was immediately circulated onto the top surface of the test plate. Water vapor condensed on the test plate surface, and droplets gradually grew. The surface temperature was constant during droplet growth, crystal growth, and frost growth stages, and the freezing time and freezing period were identified from the start of the water vapor condensation.
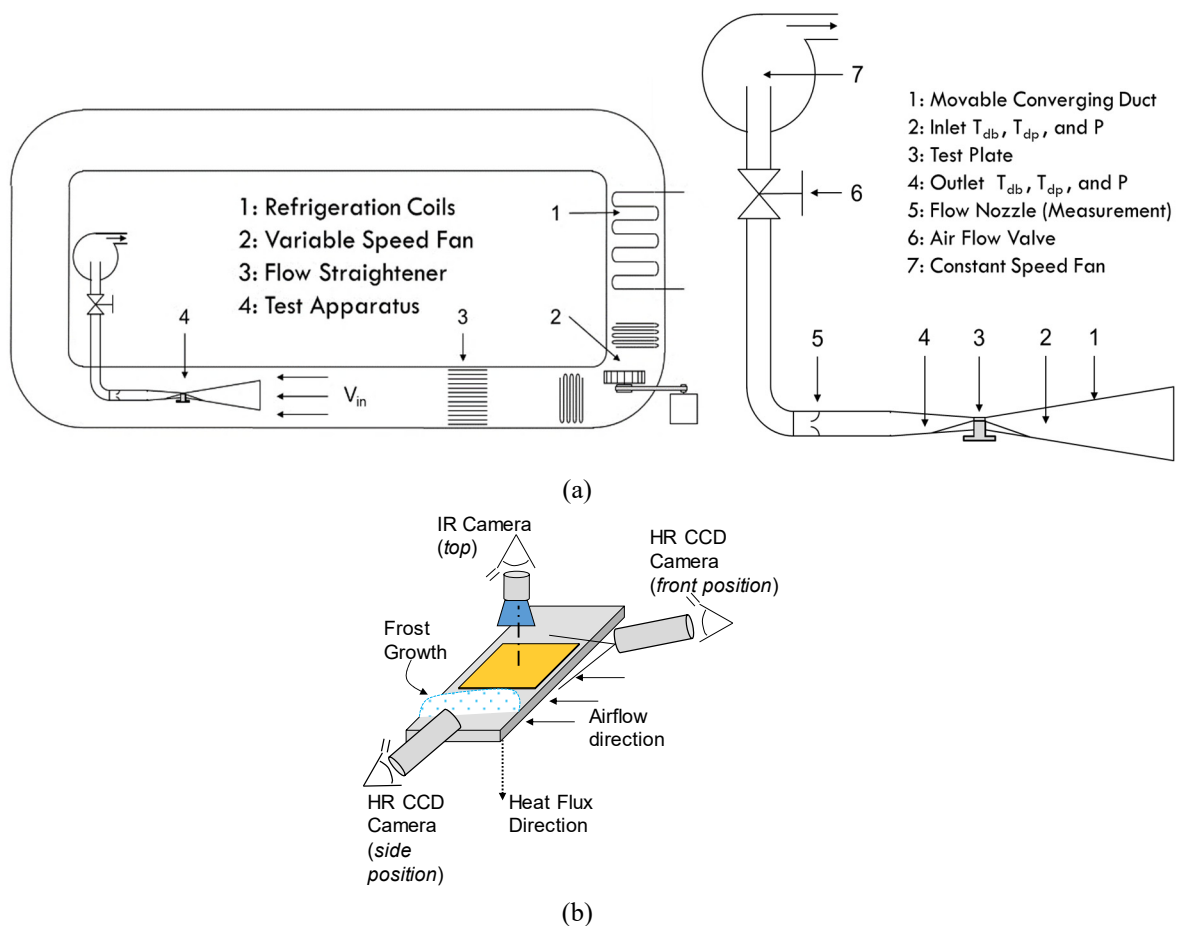

(a)

(b)

Fig. 1: (a) Schematic of main test apparatus and (b) Illustration of the HR CCD camera and IR camera with respect to the test plate.

The test plates were rectangular bars of about 6 mm (0.25 in) thickness. Four substrates and different coatings were developed, and the main body of the plates was 6061 Aluminum. While the specific details of the coatings composition are proprietary, each plate was characterized by using a static contact angle and a substrate material. The first plate (referred to as Flat Plate A) had a contact angle of about $\theta \approx 88°$. The second plate (Flat Plate B) had its top surface coated with a hydrophilic ($\theta < 10°$) coating and the third plate (Flat Plate C) had a hydrophobic ($\theta \approx 108°$) coating. These three plates shared the same substrate material. The fourth plate (Flat Plate F) had a contact angle of $\theta \approx 110°$. However, it had a different coating substrate material than the ones used in Flat Plates A, B, and C. Comparison of the data of Flat Plate F ($\theta \approx 110°$) against Flat Plate C ($\theta \approx 108°$) indicated frost nucleation characteristics for surfaces that shared same static contact angle but had different substrate materials and manufacturing processes. Twenty T-type thermocouples were embedded in the metal block underneath the test plate to measure heat flux and derive the plate's top surface temperature. The accuracy of the sensors is reported in Table 1, and the authors' previous work reported more details about the instrumentation (Cremaschi et al., 2018).

Figure 2 showed an Infrared (IR) camera image of hydrophobic flat plate C ($\theta \approx 108°$) taken during freezing at -3.8 °C (25°F) for the plate base surface temperature. The temperature color legend on the right side of Figure 2 shows the water droplets' measured temperature and iced beads in °C. The IR camera started recording and captured images every 1 frame (2 seconds = 1 frame) when water condensation first occurred on the cold test plate. In order to capture what time the freezing process occurred, the freezing duration process had to be taken into account. The "freezing duration" was defined as the time from when the first droplet was observed to begin freezing t_1 until the last droplet in the field of view of the IR camera had completed its freezing process t_2. The test started time t_0 is defined as the first instant when water droplet condensation occurred on the cold test plate. The light-colored droplets were undergoing the liquid-to-solid phase transition, that is, freezing into ice beads. They appeared lighter in color because of the temporary increase in the surrounding air temperature when the heat of fusion from the droplets was released into the surrounding air during the phase transition and the perturbation of their surface emissivity during such transition. Dark blue droplets were either still in the liquid phase or had already frozen. The details of the freezing process were discussed in detail in the authors' previous work (Harges et al. 2020).

Table 1: Measurement devices, set points, ranges, accuracies, and control tolerances

Parameter Measured	Measuring Device	Calibration	Set Point/Range	Accuracy	Control Tolerance
Sensors for controlled variables					
Air Temp. (dry bulb)	Thermocouple (grid)	In situ*	5°C (41°F)	±0.056°C (±0.1°F)	±0.28°C (±0.5°F)
Air Temp. (dew point)	Chilled Mirror Dew Point Meter	Manufacturer	0.56°C (~33°F)	±0.28°C (±0.5°F)	±0.28°C (±0.5°F)
Plate Temperature	Thermocouple (grid)	In situ*	-15°C (~5°F)	±0.04°C (±0.07°F)	±0.28°C (±0.5°F)
Air Volume Flow Rate	Flow Nozzle	Manufacturer	8.5 m³/h (~5 cfm)	±0.05 m³/h (±0.03cfm)	±0.09 m³/h (±0.05 cfm)
Measured Variables					
Air Pressure Drop	Pressure Transducer	Manufacturer	0 to 250 Pa (0 to 1″ H₂O)	0.25% full scale	(-)
Frost Surface Temperature	Infrared Camera	In situ	-22°C to 5°C (-8°F to 41°F)	±2°C (±3.6°F)	±1.6°C (±3.5°F)
Frost Mass	High Precision Digital Scale	Manufacturer	0 to 5 g (0.011 lbm)	±0.1 mg (±0.0015 gr)	(-)
Frost Thickness	CCD Camera	In-situ	0.2 to 3 mm	±80 μm @ 0.4 mm ±40 μm @ above 1 mm	
Heat Transfer Rate	Conduction side	In situ*	5 to 8 W (17 to 27.3 Btu/hr)	15%	(-)

*Temperature bath and temperature sensor with accuracy of ±0.05°C (±0.1°F) were used for on-site calibration.
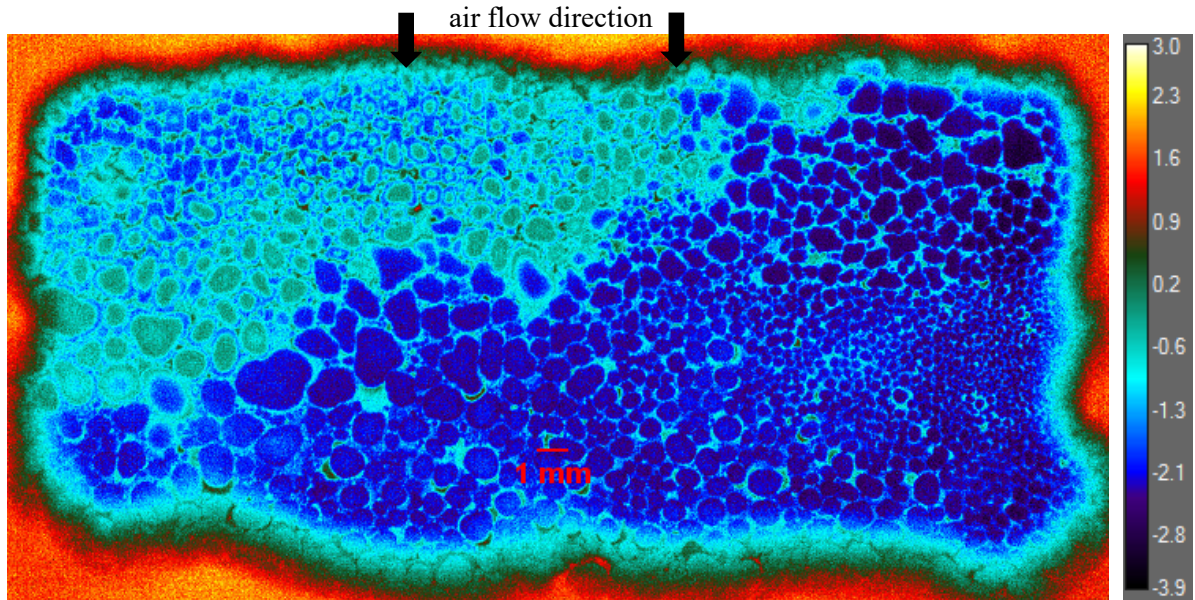
air flow direction

Figure 2: IR image of droplets freezing on the cold hydrophobic flat plate (legend color scale on the right side indicates the measured temperature with the IR camera in °C).

This single image of the freezing process in Figure 2 had an actual freezing time of about 12 minutes ($\pm$ 0.5 minutes due to human error), and it was calculated by using equation (1).

$$t_{Freezing} = (t_1 - t_0) + \left(\frac{t_2 - t_1}{2}\right) \tag{1}$$
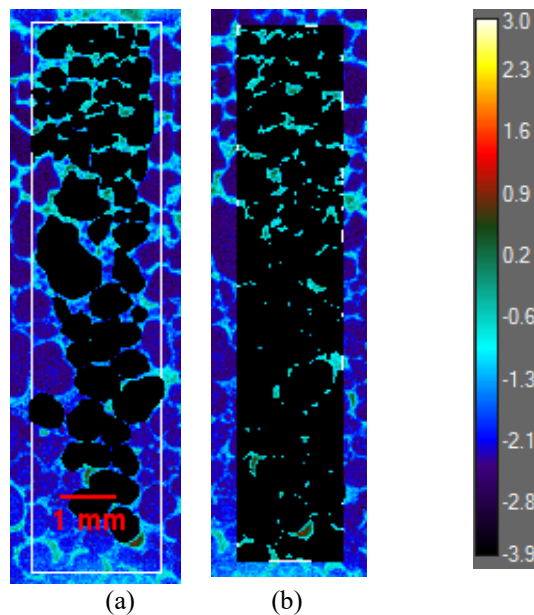

(a) (b)
Fig. 3: (a) Average diameter of water droplet measurement and (b) Average wet area coverage measurement in thermal infrared camera image (legend color scale on the right side is in °C).

The infrared camera measured the average droplet diameter and wet area coverage. Figure 3 illustrates the measurement technique of droplet size and wet area coverage. Since the droplet size looked very similar right before

and after freezing (see Figure 2), the infrared camera image shown in Figure 3 was taken from the last frame just before the first droplet was observed to begin freezing on the hydrophobic Flat Plate C ($\theta \approx 108°$) at -3.8 °C (25°F) surface temperature. The rectangular area from the top to bottom edges of the test plate was selected as the total measured area A_{tot}. The average diameter of water droplets was measured from selected droplets in Figure 3(a). The smallest droplets, which could be individually distinguished, had a diameter of about 110 μm. This size was determined based on the resolution of the IR camera and calibration of pixel size. The human error during the identification and tracing of the droplet diameters was estimated to be within 5%. The wet area A_{wet} was also measured by identification and tracing of the droplet contours, as shown in Figure 3(b). The average wet area coverage of the entire flat plate was estimated from the measured wet area in the IR camera's optical window by assuming that the ratio A_{wet}/A_{tot} was constant across the entire flat plate. In other words, the assumption of spatially uniform frost nucleation was made because the flat plate surface area was large enough to limit edge effects.

Several repeated tests for each flat plate were conducted in the present work. In these repeated tests, the environmental conditionds, surface temperature, and type of coating were identical. For Flat Plate A ($\theta \approx 88°$) and Flat Plate C ($\theta \approx 108°$), 9 tests were conducted at the same test conditions. For Flat Plate B ($\theta < 10°$), 5 repeated tests were conducted. For Flat Plate F ($\theta \approx 110°$), 7 repeated tests were conducted at the same test conditions, while 4 repeated tests were conducted at a lower plate temperature.

3. TEST RESULTS

3.1 Test conditions and repeat test freezing time results for each Flat Plate

Table 2 presents the nominal test conditions and legend numbers investigated in this study. The only difference between the two sets of test conditions is the surface temperature. For the first set of test conditions, the authors did a series of continually repeated tests on all four flat plates, while for the second test condition, only Flat Plate C ($\theta \approx 108°$) and Flat Plate F ($\theta \approx 110°$) were tested. At a surface temperature of 25°F, there were some tests for which the droplets did not freeze within 1.5 hours, especially on Flat Plate F ($\theta \approx 110°$). In order to more thoroughly analyze the frost nucleation characteristics for Flat Plate F ($\theta \approx 110°$), a second test condition was added for the comparison of Flat Plate F ($\theta \approx 110°$) and Flat Plate C ($\theta \approx 108°$).

Table 2: Test conditions and legend numbers

Test Conditions Number	1	2
Test Plate Temperature, °C (°F)	-3.8 (25)	-5 (23)
Relative Humidity, %	82%	82%
Air Temperature, °C (°F)	5 (41)	5 (41)
Air Face Velocity, m/s (fpm)	3.8 (750)	3.8 (750)

Figure 4 presents freezing times for each repeated test on all flat plates at test conditions 1. Some of the repeated tests did not freeze within one hour of testing, and those tests were not included in Figure 4. Flat Plate B ($\theta < 10°$) had the lowest average freezing time and most stable freezing time during 5 repeated tests. Flat Plate A ($\theta \approx 88°$) and Flat Plate C ($\theta \approx 108°$) had unstable and somewhat inconsistent freezing time within the 9 repeated tests. Flat Plate C ($\theta \approx 108°$) had two trials that did not freeze within one hour; those tests were excluded from Figure 4 and were not included in the freezing time average. But the poor repeatability and large freezing times of Flat Plate A ($\theta \approx 88°$) and Flat Plate C ($\theta \approx 108°$) are still reported in this figure to clearly show the contrast to the data of Flat Plate B ($\theta < 10°$). The first repeat test of Flat Plate C ($\theta \approx 108°$) was excluded because its freezing time was over 1 hour, while the third repeat test of Flat Plate C ($\theta \approx 108°$) had a freezing time of around 13 minutes only. This inconsistent freezing results might be caused by high test surface temperature had low dependence on surface wettability.

As a reminder, Flat Plate F ($\theta \approx 110°$) had a very close contact angle to Flat Plate C ($\theta \approx 108°$), but Flat Plate F ($\theta \approx 110°$) had a different coating substrate. Unlike Flat Plate A ($\theta \approx 88°$) and Flat Plate C ($\theta \approx 108°$), there was only one test on Flat Plate F ($\theta \approx 110°$) which froze within one hour of testing. All other repeated tests on Flat Plate F ($\theta \approx 110°$) were unfreezing within two-hour test periods. Thus, it was challenging to compare Flat Plate F ($\theta \approx 110°$) with other test plates in Figure 4 with respect to freezing time. Analysis of the average droplet size at the same test run time was still possible for all tested flat plates. The details of the droplets IR images will be shown and discussed in the next section.
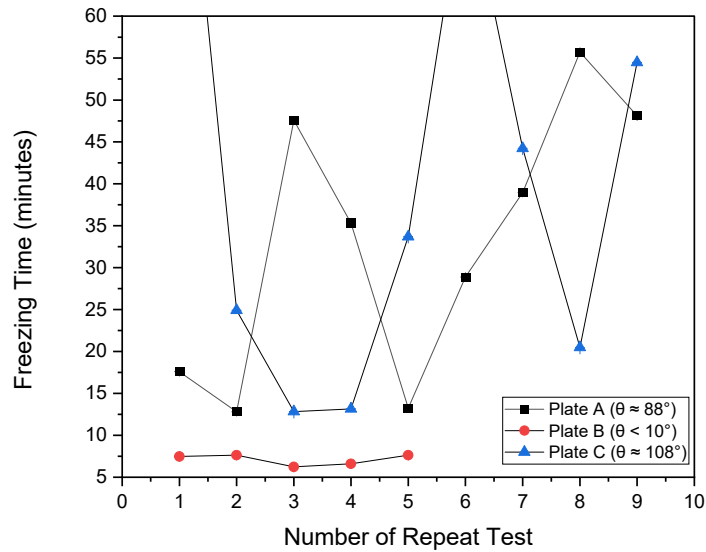
Figure 4: Freezing time vs. number of repeat tests for Flat Plate A ($\theta \approx 88°$), Flat Plate B ($\theta < 10°$) and Flat Plate C ($\theta \approx 108°$) under test conditions 1. ($T_s = 25°F$, $T_{a,in} = 41°F$, $\omega_{in} = 80\%$ R.H., $V_a = 3.8$ m/s)
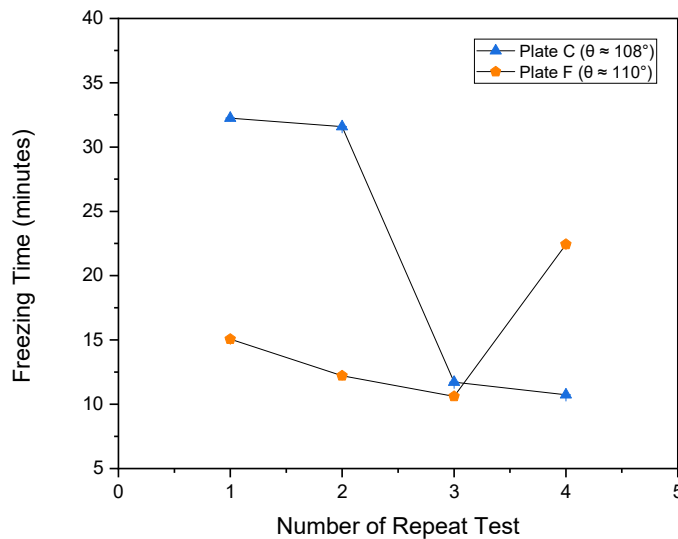

Figure 5: Freezing time vs. number of repeat tests for Flat Plate C ($\theta \approx 108°$) with coating substrate type 1 and Flat Plate F ($\theta \approx 110°$) with coating substrate type 2 under test conditions 2. ($T_s = 23°F$, $T_{a,in} = 41°F$, $\omega_{in} = 80\%$ R. H., $V_a = 3.8$ m/s)

Figure 5 presents freezing times for Flat Plates C ($\theta \approx 108°$) and F at test conditions 2. For test conditions 2, the surface temperature was reduced to 23°F, and four repeated tests were performed for the different flat plates. Compared to Flat Plate C ($\theta \approx 108°$), Flat Plate F ($\theta \approx 110°$) had less variability of the freezing time and, in average, it had a shorter freezing time. That shows that the surface wettability of Flat Plate F ($\theta \approx 110°$) had a significant effect on freezing time in this series of repeat tests.

From a literature review study, researchers (Kim et al. 2016, Zhang et al. 2016, Wang et al. 2014.) pointed out that surface wettability can delay the freezing time. Harges et al. (2020) showed that when relatively high sub-freezing

plate temperatures were used, the test plates' surface wettability had a minor impact on the freezing time. The authors' previous work also highlighted that minor surface imperfections could inhibit the surface wettability effect and delay freezing. When comparing two different surface temperature test conditions, it was observed that Flat Plate C ($\theta \approx$ 108°) had a more coherent freezing time region when its surface temperature was 23°F. Flat Plate C ($\theta \approx$ 108°) had inconsistent freezing times at the higher surface temperature, and the root causes of this behavior are unclear and require further investigation. In particular, analysis of this surface before and after multiple frost and defrost processes could shed some light on potential surface modifications and contamination affecting the freezing time during the run time at 25°F.

3.2 Average Freezing Time Results and Frozen Droplet Characteristics

Table 3 presents the average freezing time and average droplet diameter at the time of freezing for all flat plates and test conditions. Flat Plate B ($\theta < 10°$) had the lowest freezing time. Even though Flat Plate A ($\theta \approx 88°$) had a similar freezing time to Flat Plate C ($\theta \approx 108°$), it still had a different average frozen droplet diameter. Flat Plate C ($\theta \approx 108°$) had the lowest average droplet diameter, and the size of the droplets on Flat Plate C ($\theta \approx 108°$) was pretty small. The average freezing time of all cold flat plates was dependent on surface temperature. The average diameter of Flat Plate C ($\theta \approx 108°$) did not change significantly if its surface temperature decreased from 25°F to 23°F. In comparison, Flat Plate F ($\theta \approx 110°$) showed that if the surface temperature dropped, the droplet sizes were measurably different. Thus, the various substrates of the coating of Flat Plate F ($\theta \approx 110°$) affected droplet size and shape, but such effect was measurable when the surface temperature was equal to or above 25°F.

Table 3 Average Freezing time and frozen droplet diameter for each flat plates and each set of test conditions

Surface Temp.	Flat Plate A ($\theta \approx 88°$)		Flat Plate B ($\theta < 10°$)		Flat Plate C ($\theta \approx 108°$)		Flat Plate F ($\theta \approx 110°$)	
	t_s (min)	Diameter (mm)	t_s (min)	Diameter (mm)	t_s (min)	Diameter (mm)	t_s (min)	Diameter (mm)
25°F	33	1.26 ± 0.1	7	1.19 ± 0.1	29	0.98 ± 0.1	24	2.14 ± 0.1
23°F	Not Tested	Not Tested	Not Tested	Not Tested	21	0.92 ± 0.1	15	1.11 ± 0.1

Figure 6 presents droplet IR images for the droplet's size and shape on each flat plate. The image for Flat Plate B ($\theta < 10°$) was taken at about 7 minutes after the surface was exposed to humid airflow, while the images for Flat Plates B, C, and F were taken at about 12 to 13 minutes of continuous exposure to the air. In all cases, the surfaces were set at a temperature of 25°F. The droplets on Flat Plate B ($\theta < 10°$) had the largest average diameter among all test flat plates. Because of superhydrophilic wettability properties, the droplets spread out to wet much of the test plate and had irregular shapes. Flat Plate A ($\theta \approx 88°$) had a low contact angle and presented irregular droplet shapes. Flat Plate C ($\theta \approx 108°$) had the same coating base with Flat Plate A ($\theta \approx 88°$) but a larger contact angle. Flat Plate C ($\theta \approx 108°$) showed the same irregular droplet shape as Flat Plate A ($\theta \approx 88°$). But droplets on Flat Plate C ($\theta \approx 108°$) were smaller and appeared more similar. On the contrary, droplets on Flat Plate A ($\theta \approx 88°$) were sparser than on Flat Plate C ($\theta \approx 108°$) and Flat Plate F ($\theta \approx 110°$). Flat Plate F ($\theta \approx 110°$) had a similar contact angle to that on Flat Plate C ($\theta \approx 108°$) but a different coating substrate component. Droplets on the Flat Plate F ($\theta \approx 110°$) appeared to have the same irregular shape as Flat Plat C but of larger size and a more uniform droplet size distribution.

It should be noted that the droplet sizes in Figure 6 do not necessarily have to match the average droplet diameter in Table 3. Flat Plate A ($\theta \approx 88°$) and Flat Plate F ($\theta \approx 110°$) had similar diameters at 12-13 minutes, while for the frozen droplet average diameter after 24 minutes, the Flat Plate F ($\theta \approx 110°$) showed the largest droplets size in Table 3. It was expected that larger diameter droplets would be obtained when the surface contact angle decreased (Hoke et al., 2000). However, for the flat plate types investigated in the present work and for the plate temperatures well below the freezing point as in Figure 6, the surface wettability effects on droplet shape were not as marked as suggested in some of the studies in the literature. In Table 3, comparing Flat Plate F ($\theta \approx 110°$) and Flat Plate C ($\theta \approx 108°$) under the lower surface temperature test condition, the measured average diameters were quite similar.
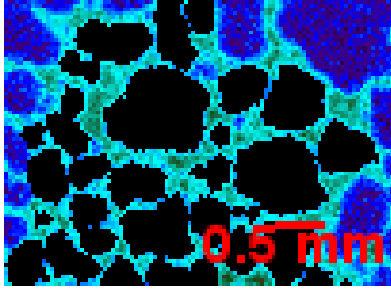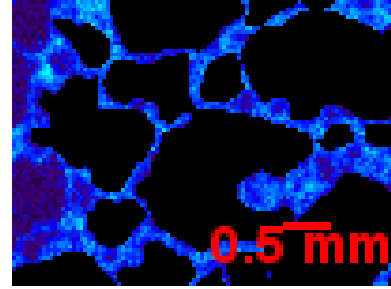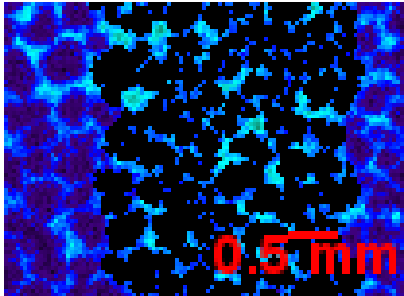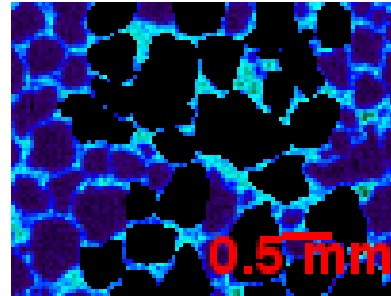
(a) Flat Plate A ($\theta \approx 88°$), Average Diameter = 0.57 mm

(b) Flat Plate B ($\theta < 10°$), Average Diameter = 1.19 mm

(c) Flat Plate C ($\theta \approx 108°$), Average Diameter = 0.27 mm

(d) Flat Plate F ($\theta \approx 110°$), Average Diameter = 0.57 mm

Figure 6: Average droplet diameter and droplet shape on a different flat plate with a hydrophilic and hydrophobic coating. Flat Plate B ($\theta < 10°$) was taken at freezing time around 7 minutes under -3.8°C (25°F) surface temperature; images for Flat Plate A ($\theta \approx 88°$), Flat Plate C ($\theta \approx 108°$), and Flat Plate F ($\theta \approx 110°$) with coating substrate type 2 were taken around 12-13 minutes.

3.3 Droplets area coverage
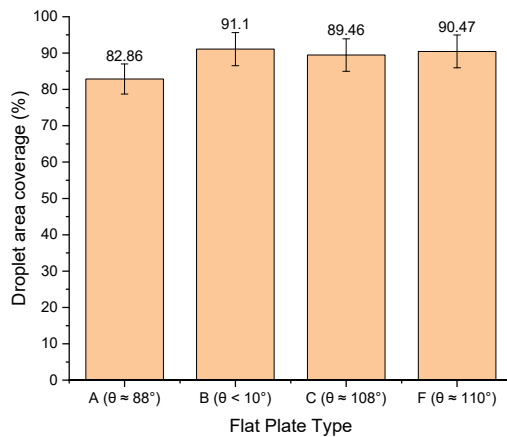
(a)
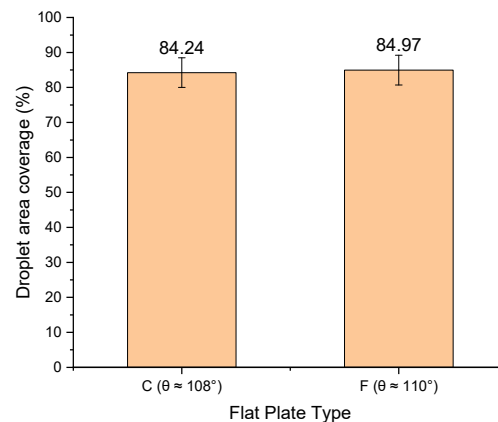
(b)

Figure 7: Average droplet area coverage vs different surface wettability. (a) 25°F Surface temperature test condition. (b) 23°F Surface temperature test condition.

Figure 7 shows the average droplet area coverage with different surface wettability and different surface temperature. As a reminder, all the droplet area coverage showed in Figure 7 was measured at freezing time. Flat Plate B ($\theta < 10°$) had the most significant droplet area coverage than other hydrophobic test plates. Flat Plate A ($\theta \approx 88°$) had the lowest droplet area coverage. From the literature study, the lower cold substrate surface temperature was expected to augment

the area coverage (Sheng et al., 2020). However, Flat Plate C (θ ≈ 108°) and Flat Plate F (θ ≈ 110°) had the opposite trend and, as indicated in Figure 7, the droplet area coverage decreased by about 5% if surface temperature fell from 25 to 23°F. Because the droplets on Flat Plate C (θ ≈ 108°) were pretty tiny at the beginning and pinned on the surface with a visible high density, when such droplets grew, the droplet area coverage increased. At 25°F, the droplets remained in the water phase for a longer time, and this more extended condensation period allowed more moisture vapor to accumulate on the cold plate. As a result, Flat Plate C (θ ≈ 108°) and Flat Plate F (θ ≈ 110°) had more extensive wet area coverage at their freezing time if their surface temperature was 25°F, that is, closer (but still below) the water triple point temperature.

4. CONCLUSIONS

This paper presented new experimental data of ice droplets nucleation and water droplet characteristics on cold flat plates operating in frosting conditions and with air-forced convective flow. Four test flat plates with different wettability were investigated under two testing conditions. The contact angle ranged from less than 10° (i.e., superhydrophilic) to over 109° (i.e., hydrophobic). Two test flat plates shared similar contact angles but had different substrates of the coatings.

The average freezing times for the cold flat plates investigated in the present paper depended on their surface temperatures. Superhydrophilic Flat Plate B (θ < 10°) had the shortest freezing time, and it ranged between 6 and 7 minutes. Flat Plate A (θ ≈ 88°) and Flat Plate C (θ ≈ 108°) had longer freezing times than the superhydrophilic coated Flat Plate B. Repeated tests of Flat Plate A (θ ≈ 88°), C (θ ≈ 108°) showed that freezing time had large fluctuations, ranging from 13 up to 56 minutes. However, if surface temperature decreased by only a few degrees, then a much narrower span of freezing times was observed.

Iced droplet sizes and area coverage were also measured and discussed in this paper. The superhydrophilic Flat Plate B (θ < 10°) had large droplets spread out on the surface. The droplets on the hydrophobic Flat Plate C (θ ≈ 108°) had the smallest size, and ample wet area coverage, and the diameter did not change significantly if surface temperature decreased from 25°F to 23°F. The same was not valid for Flat Plate F (θ ≈ 110°), which showed that if surface temperature decreased, the droplet sizes were measurably different. Thus, for temperatures slightly below the freezing point, the various substrates combined with the top coatings affected droplet size and shape before the onset of freezing. The IR images of the present work showed that the static contact angle of the surface had a weak effect on the shape of the droplets before they turned into iced beads. For a similar contact angle of θ ≈ 108° to 110°, the substrate had a measurable effect on the droplet diameter when the surface temperature was at least 25°F or above. Hydrophobic surfaces investigated in the present work showed somewhat irregular splattered droplet shapes. This intriguing visual observation from the IR images appeared not consistent with the data shown in some literature studies (for example, in Harges et al. 2020). It might be due to differences in the specific surface coating chemistry and substrate materials of the flat plate investigated in the present work. Further investigations should be conducted in future research before comparing the droplet shapes from surfaces with similar static contact angles with different chemistry of the coatings.

NOMENCLATURE

A_{wet}	Droplet covered wet area	
A_{tot}	The selected total area for droplet measurement	
t_s	Freezing time	(minutes)
T	temperature	(F)
$\dot{V}$	volume flow rate	(m³/h)
ω	absolute humidity ratio	(kg_water vapor/kg_dry air)
θ	surface contact angle	(degree)
Subscript		
a,	air	
in	inlet of the test section	
out	outlet of the test section	

REFERENCES

Tao, Y.-X., Besant, R. W., Mao, Y., 1993. Characteristics of frost growth on a flat plate during the early growth period. *ASHRAE Transactions 99*, pp. 746-753. NAID: 10018602651

Sheng, W., Pei, Y., Li, X., Ming, P. and Zhao, W., 2020. Effect of surface characteristics on condensate droplets growth. *Applied Thermal Engineering*, p.115260

Kim, H., Kim, D., Jang, H., Kim, D.R. and Lee, K.S., 2016. Microscopic observation of frost behaviors at the early stage of frost formation on hydrophobic surfaces. *International Journal of Heat and Mass Transfer*, *97*, pp.861-867.

Hoke, J.L., Georgiadis, J.G. and Jacobi, A.M., 2000. *The interaction between the substrate and frost layer through condensate distribution*. Air Conditioning and Refrigeration Center. College of Engineering. University of Illinois at Urbana-Champaign. uri: 2142/12004

Seki, N., Fukusako, S., Matsuo, K. and Uemura, S., 1985. An analysis of incipient frost formation. *Wärme-und Stoffübertragung*, *19*(1), pp.9-18.

Bryant, J., 1995. *Effects of hydrophobic surface treatments on dropwise condensation and freezing of water* (Doctoral dissertation, Texas A&M University). uri: 1969.1/154822

Kim, D., Kim, H., Kim, S.W., Kim, D.R. and Lee, K.S., 2015. Experimental investigation of frost retardation for superhydrophobic surface using a luminance meter. *International Journal of Heat and Mass Transfer*, *87*, pp.491-496.

Cremaschi, L., Harges, E., Adanur, B., Strong, A., 2018. Frost nucleation and frost growth on hydrophobic and hydrophilic surfaces for heat exchangers fin structures. *International Refrigeration and Air Conditioning Conference*, Paper 1994. docs.lib.purdue.edu/iracc/1994/

Adanur, B., Cremaschi, L., Harges, E., 2019. Effect of mixed hydrophilic and hydrophobic surface coatings on droplets freezing and subsequent frost growth during air forced convection channel flows. *Science and Technology for the Built Environment 25*(10), pp. 1302-1312. doi: 10.1080/23744731.2019.1648981

Harges, E., 2019. Cremaschi, L., Adanur, B., 2020, Distribution, Coalescence, and Freezing Characteristics of Water Droplets on Surfaces with Different Wettabilities under Subfreezing Convective Flow. *Applied Thermal Engineering,* p.116052

Zhang, H.F., Zhao, Y.G., Lv, R., Yang, C.. 2016, freezing of sessile water droplet for various contact angles. *International Journal of Thermal Sciences*, pp.59-67. 1290-0729.

Wang, Z.J., Kwon, D.J., L. DeVries, K., Park, J.M. 2014. Frost formation and anti-icing performance of a hydrophobic coating on aluminum. *Experimental Thermal and Fluid Science.* page 132-137, 0894-1777.

ACKNOWLEDGEMENT